TWENTYFIFTH EUROPEAN ROTORCRAFT FORUM

Paper n° B7

The ERATO Programme: Wind Tunnel Test Results and Proof of Design for an Aeroacoustically Optimised Rotor

by

W. R. Splettstoesser, B. van der Wall, B. Junker, K.-J. Schultz
DLR, Braunschweig, Germany

and

P. Beaumier, Y. Delrieux, P. Leconte
ONERA, Châtillon, France
P. Crozier
ONERA, Modane, France

September 14 - 16, 1999
Rome
Italy

ASSOCIAZIONE INDUSTRIE PER L'AEROSPAZIO, I SISTEMI E LA DIFESA
ASSOCIAZIONE ITALIANA DI AERONAUTICA ED ASTRONAUTICA

The ERATO Programme: Wind Tunnel Test Results and Proof of Design for an Aeroacoustically Optimised Rotor

W. R. Splettstoesser, B. van der Wall, B. Junker, K.-J. Schultz
DLR, Braunschweig, Germany

and

P. Beaumier, Y. Delrieux, P. Leconte
ONERA, Châtillon, France
P. Crozier
ONERA, Modane, France

Abstract

The bilateral ERATO project between ONERA and DLR had the ambitious goal to design, build, and test a quiet model rotor which is 6 dB less noisy in specific descent and level flight conditions than a reference rotor of current technology (the 7AD ONERA-EC rotor), for a helicopter of the 4 to 6 ton class with the constraints of minimum power and vibration level penalties. This cooperative research effort resulted in a novel aeroacoustically optimised rotor blade design, which was built with extensive pressure and strain gauge instrumentation. Both the ERATO and the 7AD rotor have been tested in the S1 Modane-Avrieux (S1MA) wind tunnel (acoustically lined closed test section) at high-speed and in the DNW (open jet anechoic test section) at moderate and low speed to prove compliance with the objectives and to verify the design methodology employed. The results of both test campaigns together with a preliminary analysis are presented and the noise reduction potential at simultaneously improved performance of the ERATO rotor in comparison to the reference rotor is demonstrated.

The novel quiet rotor features acoustic gains up to 7 dBA at descent flight and up to 13 dBA at high speed level flight. Furthermore, significant rotor performance gains (up to 12 %) were found for high speed level flight, but limited to moderate blade loadings. In summary, the high quality experimental results globally verify the quiet rotor design methodology applied.

1 Introduction

Blade-Vortex Interaction (BVI) impulsive noise continues to be a source of major concern near heliports and landing pads. The reduction of BVI impulsive noise is still a challenge for improving the acceptability of rotorcraft. In the past few years, a number of highly sophisticated experimental investigations conducted in aeroacoustic wind tunnels have substantially improved the knowledge on BVI noise generation and have furthered the physical insight into this aeroacoustic phenomenon. In parallel efforts taking advantage of the newly created quality data bases, the aerodynamic and acoustic prediction tools have significantly been amended (refs 1,2,3,4).

Previously, attempts have been made to reduce BVI impulsive noise by cleverly shaping the blade tip geometry or by employing sub-wings or spoilers, however, with only marginal success (refs 5,6). More recently, active blade (root) control (ABC) concepts, like HHC or IBC have successfully been tested in model-scale and full-scale with significant noise reduction benefits of up to 6 dBA (refs 7,8,9). Presently, different ABC concepts, like servo flaps, direct lift flaps, and direct twist are being investigated partly making use of so-called smart materials (ref 10).

In an alternative, bilateral effort (of ONERA and DLR) a new attempt was made to reduce BVI impulsive noise by passive means, i.e. by aeroacoustically optimising the blade geometry and thus reducing the noise generation at its very source. A survey on this bilateral research programme between DLR and ONERA called ERATO is given in reference 11. ERATO is an acronym for "Etude d'un Rotor Aeroacoustique Technologiquement Optimal" and stands for aeroacoustic rotor optimization. This paper is particularly devoted to results of the wind tunnel validation tests and proof of design of the novel aeroacoustically optimised model rotor.

The ambitious goal of the ERATO programme was to design, build, and test a quiet model rotor which is 6 dB less noisy in specific descent and level flight conditions than a reference rotor of current technology (the ONERA-EC 7AD rotor) for a helicopter of the 4–6 ton class with the constraints of minimum power and vibration level penalties. Moreover, for level flight at moderate speed (215 km/h) and high

Presented at the 25th European Rotorcraft Forum, Rome, Italy, September 14 - 16, 1999

speed (350 km/h) a significant acoustic benefit was envisaged.

The ERATO programme was realised in three phases jointly by DLR and ONERA with some guidance provided by EC and ECD. In an exploratory phase, the aerodynamic and acoustic codes have been upgraded and validated by making use of existing experimental data (ref 8). The main phase comprised extensive parametric studies, the choice of an initial blade design, and the optimisation of this initial design under consideration of the given constraints. In the final validation phase of the programme, the optimised, highly instrumented model rotor was built and subsequently tested in both the S1MA wind tunnel (fitted with acoustic lining) in the high speed range up to 350 km/h (190 kts) for performance and acoustics and in the DNW aeroacoustic test section in the low-to-moderate airspeed range of 70 to 260 km/h (38 to 140 kts) for acoustics and performance as well.

The present paper is focussed on these validation tests and reports on initial results obtained in both tunnels, where simultaneous measurements of blade surface pressures, acoustic radiation and rotor performance were conducted in order to assess the noise reduction potential of the novel ERATO rotor in comparison to the reference rotor. The tests in the DNW were supplemented by non-intrusive flow field measurements, like LLS and PIV and another optical measurement technique, called PGM, to provide a better physical insight into the rotor wake behaviour and the blade aeroelastic deflections, respectively.

2 Experimental Approach

The Mach-scaled model rotor tests were conducted in different wind tunnels (DNW and S1MA) to take advantage of the different flow velocity and aeroacoustic capabilities of each facility. Consequently, two individual test plans were developed to meet the test objectives planned for each tunnel entry. The common features like rotor characteristics, instrumentation and trim are described below, while the features specific for the two test series are given in separate chapters.

Rotor Characteristics and Instrumentation: Both 4-bladed, 4.2 m-diameter rotors have a mean blade chord c of 0.14 m and a solidity • of 0.085 in common, but differ in twist, airfoil distribution and planform. The 7AD blade features -8.3°/R twist, 0A2xx series airfoil distribution and a parabolically swept back tip with 12.5° anhedral. The ERATO blade comprises -10°/R twist, 0A3xx and 0A4xx series airfoil distribution, and a planform with forward and backward sweep of the quarter chord line and a straight tip (not optimised). The planform for both rotors indicating the pressure instrumented sections are depicted in Fig. 1. The instrumentation of the optimised ERATO rotor comprised 124 absolute pressure sensors of the piezoresistive type (Kulite LQ33) and 32 strain gauges, while the reference rotor was equipped with 118 pressure sensors (Kulite XCQ) and 28 strain gauges.

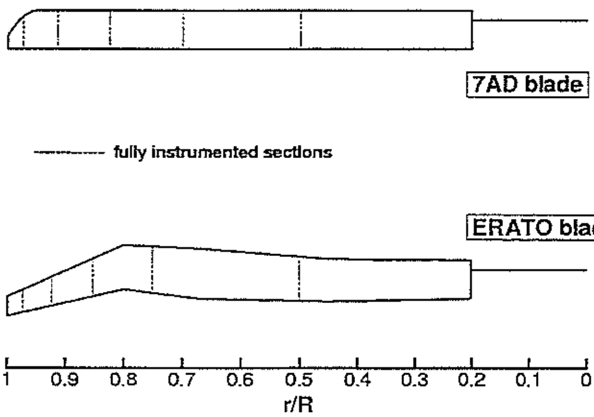

Fig. 1: Planform of the reference rotor (7AD) and of the optimised rotor (ERATO).

Rotor Trim Procedure: To attain meaningful results for the comparison of the acoustic and aerodynamic data of the two different rotors, the force trim procedure was chosen and used to trim the model rotors as closely as possible to a full-scale helicopter in free flight. Lift and propulsive force coefficients had been pre-calculated for a given helicopter mass M, fuselage drag D and flight condition (velocity V_∞ and flight path angle •). At first, non-dimensional helicopter weight coefficient $Z_W{}^*$ and fuselage drag coefficient $C_dS_f / (S\sigma)$ were defined by

$$Z_W{}^* = 200\, M \bullet g \,/\, (\bullet \bullet S \bullet \bullet\bullet (R \bullet^*)^2)$$
$$C_dS_f / (S\sigma) = D \,/\, (0.5 \bullet\bullet \bullet V_\infty{}^2)$$

Where σ is rotor solidity, • is air density, S and S_f are rotor disc and fuselage drag planes. • * is a reference rotor angular velocity. Then, the lift coefficient $Z_b{}^*$ and the propulsive force coefficient $X_b{}^*$ expressed in the wind tunnel coordinate system are defined by

$$Z_b{}^* = Z_W{}^* \cos \bullet$$
$$X_b{}^* = -(Z_W{}^* \sin \bullet + 100\, \mu^{*2}\, C_dS_f / (S\sigma))$$

with advance ratio $\mu^* = V_\infty / (R \bullet^*)$. The $Z_b{}^*$ and $X_b{}^*$ coefficients were matched very closely during the wind tunnel tests. The rotor hub drag was determined prior to the test and subtracted from the force measurements. Wind tunnel wall corrections (Brooks/Burley) have been calculated online (negative for the DNW open test section) and been applied in the trim procedure. Collective and cyclic pitch and rotor shaft tilt were employed to trim the rotor to the prescribed lift and propulsive forces and to the selected blade flapping law, mainly zero flapping (American law) in the DNW as well as zero flapping and a special Modane law in the S1MA tunnel.

2.1 Tests in S1MA

Test set-up: The helicopter rotor test rig of the S1MA wind tunnel (Fig. 2) consists of a four-leg structure supporting a mechanism able to tilt the rotor shaft from 25^0 (backward) to 95^0 (forward). The torque (7000 Nm max. at 680 RPM) is provided by a 500 kW drive unit and transmitted to the rotor through a non rotating 6-component balance. A torque meter enables to calculate the rotor performance. The test section is 8 m in diameter and 14 m in length. Though the test section was originally not designed for aeroacoustic tests, two kinds of acoustic lining can optionally be implemented: one is able to sustain flow velocities up to 1000 km/h, another, more adapted to helicopter studies, can be used up to 400 km/h. Consequently, the test section walls were fitted with the latter acoustic lining which has an absorption coefficient under normal incidence larger than 0.9 above 400 Hz (that is above the sixth harmonic of the bpf). Ten ¼-inch AKSUD microphones mounted with nose cones were installed to serve for the acoustic measurements. Two of them were mounted on the walls in the rotor plane: one on the advancing blade side, the other one on the retreating side. The eight other microphones were distributed along a vertical strut located 3 rotor radii upstream of the rotor hub, in the test section symmetry plane. The upper microphones (near the rotor plane) were intended to measure more particularly the high-speed impulsive noise, the lower ones to measure the loading (including BVI) noise.

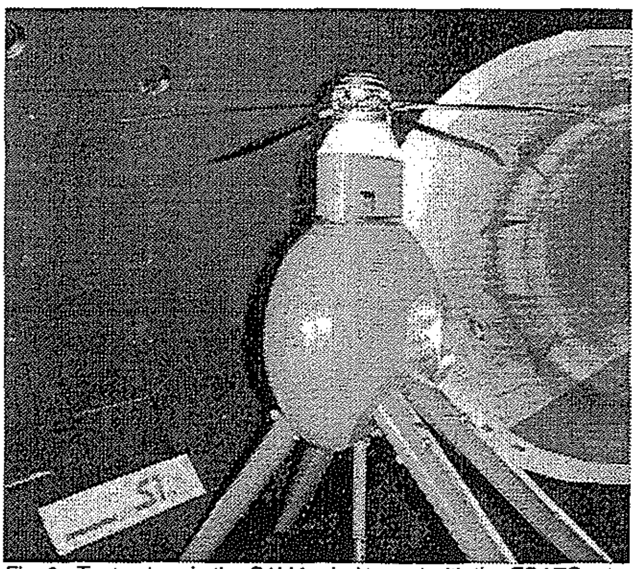

Fig. 2: Test set-up in the S1MA wind tunnel with the ERATO rotor installed.

Data acquisition and processing: The blade pressures were acquired in synchronisation with the rotor at the rate of 256 per rev., amplified in the rotating frame, multiplexed and transmitted to the fixed frame through a slip-ring assembly. Then the signals were averaged over 30 successive revolutions. A chordwise integration of the pressures at the fully instrumented sections provided the corresponding sectional lifts. The microphone signals were also acquired in synchronisation with the rotor at the rate of 1024 per rev, which yield a useful frequency of 8 kHz at the nominal rotation speed for the analysis of the acoustic data. The sound pressure time signatures were ensemble-averaged on three hundred successive rotor revolutions. Noise levels in dBA (transposed to a scale-one rotor) have been calculated. Furthermore, the time signatures have been filtered in the 6^{th} to 40^{th} bpf frequency band for the needs of the physical analysis comprising both the removal of remaining low frequency tunnel wall reflections and the identification of the BVI noise contribution.

Test conditions: Both rotors have been tested at the moderate-to-high speed level flight conditions with variation of

- flow Mach number (M_∞) from 0.175 to 0.286
- advance ratio (μ^*) from 0.283 to 0.463
- rotational tip Mach number ($M_{\Omega R}$) from 0.573 to 0.661
- weight coefficient (Z_W^*) from 10 to 17.5
- drag coefficient $C_dS_f/S\sigma$ from 0.07 to 0.15.

2.2 Tests in the DNW

After completion of the measurement programme for the moderate-to-high speed range of the flight envelope in S1MA, the experimental programme was continued in the open-jet, anechoic test section of the DNW focussed on the low-to-moderate speed range of the flight envelope with emphasis on descent flight conditions known to generate extensive BVI noise.

Test Set up: The open-jet configuration employed an 8 m by 6 m nozzle that provides a 19-m-long free jet with a low-turbulence potential core. In Fig. 3 the DLR model rotor test stand mounted on the DNW sting is shown together with the traversing in-flow microphone array which was placed 2.3 m underneath. The test rig fuselage, sting and traverse were acoustically treated to minimize reflections. The test rig essentially consisted of a support mounted 6-component balance, measuring both static and dynamic rotor forces and moments. On the same support a hydraulic motor (130 KW) was mounted to drive the rotor shaft via a flexible belt. By this arrangement a hollow shaft was provided for the instrumentation cabling of the rotating system. All sensor output signals of the rotating frame were fed through the rotor shaft into a computer controlled miniature amplifier unit for proper pre-amplification before transmission to the fixed frame via a slipring assembly.

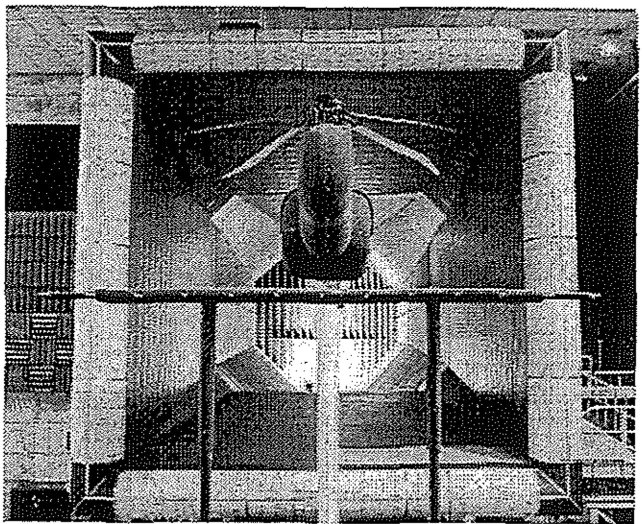

Fig. 3: Test set-up in the DNW open-jet test section with ERATO rotor mounted.

Data Acquisition: The emitted rotor noise was measured by 13 movable and 2 stationary 1/2 - inch microphones of the pressure response type mounted with nose cones. The movable microphones of the in-flow array were arranged symmetrically and spaced 0.45 m apart on a horizontal wing (Fig. 3). The array was traversed about 4 m upstream and 4 m downstream of the rotor hub (X-direction) creating a large horizontal measurement plane (X/R = 4, Y/R = 2.6) at a distance of Z/R = 1.1 underneath the rotor hub. From the slowly moving (33 mm/s) microphone array 30 rotor revolutions of microphone data were taken by a transputer based system at each streamwise step, 0.5 m apart. After completion of a traverse the sound field was defined by 221 individual measurement points providing an excellent spatial resolution. The 30 rotor revolutions of real-time acoustic pressure data, taken at 2048 samples per revolution, were processed on-line as well as being stored for further analysis. Bandpass filtering was used so that the useful frequency range was 20 Hz to 16 kHz. In addition to standard system calibrations, background noise and acoustic quality tests were performed. The acoustic data were evaluated in terms of mid-frequency band pass levels (L-MF) comprising the 6^{th} - 40^{th} blade passage frequency harmonics (a representative measure for BVI impulsive noise) and in terms of A-weighted and Noy-weighted levels.

A similar transputer based system with a capacity of 230 channels was used for the acquisition of the blade pressure and strain gauge data. Each of the channels was digitized at a rate of 2048 per revolution providing a useful frequency range up to 16 kHz, however, due to the specifics of the pressure transducers and their installation a flat frequency response up to 6 kHz (3 kHz for the reference rotor) have been proven, which is sufficient for the blade pressure signals. For each rotor condition 64 revolutions were sampled immediately before each microphone traverse was started and on-line processed during the acoustic data acquisition. The data acquisition was initiated when wind tunnel and rotor were reported on condition. After acquisition of the wind tunnel data and shortly before the acquisition of the blade pressure data, the rotor data were measured over a period of 32 revolutions; 96 sensor signals were digitised at 128 samples per revolution with a useful frequency content of 210 Hz. All data acquisition systems were triggered by blade position reference signals from an angle encoder. Digitised wind tunnel and rotor data were merged into a common data base.

Test conditions: The flight conditions simulated in the DNW covered a major part of a helicopter flight envelope focussed on low-to-moderate speed descent (BVI conditions) and level flight and included also two climb conditions, with variation of

- flow Mach number from 0.059 to 0.212
- advance ratio from 0.095 to 0.344
- rotational tip Mach number from 0.573 to 0.661
- weight coefficient from 12.5 to 17.5
- drag coefficient $C_d S_f / S\sigma = 0.1$
- flight path angle (φ) from +12° (climb) to -12° (descent)

LLS Flow Visualisation: The Laser Light Sheet (LLS) technique (ref 12) was applied to visualise tip vortex sections in order to attain quantitative information on the geometry of tip vortex segments and on the blade-vortex miss distance at locations of severe BVI. Such information is important to validate or improve the free wake code used in the noise prediction calculation chain.

PIV Measurements: The objectives of the 2D - Particle Image Velocimetry (PIV) measurements were to attain vortex strength and core size of the vortices interacting intensively with the rotor blades on the advancing side near 55° azimuth. This was accomplished by measuring the vortex velocity fields within a window of about 0.2 m by 0.16 m, which was placed within a vertical plane orientated at 45° towards the tunnel flow. The principal set-up of the PIV measuring device is illustrated in Fig. 4. Details of the PIV measuring technique are given in ref 13.

Blade Deflection Measurements: Aeroelastic blade deflections, especially torsional and flapwise deflections represent important parameters affecting BVI noise and vibrations. Two different techniques were applied to obtain the required information. The first one was the conventional strain gauge techniques, which made use of the torsional, flapwise and inplane deflections along the blade span. This technique provides results for all azimuth angles, but the deflections are generally coupled to a certain degree. The accuracy may be improved by adjustments based on the Projected Grid Method (PGM) developed for application by DNW (ref 8). However, PGM data analysis has not yet been completed.

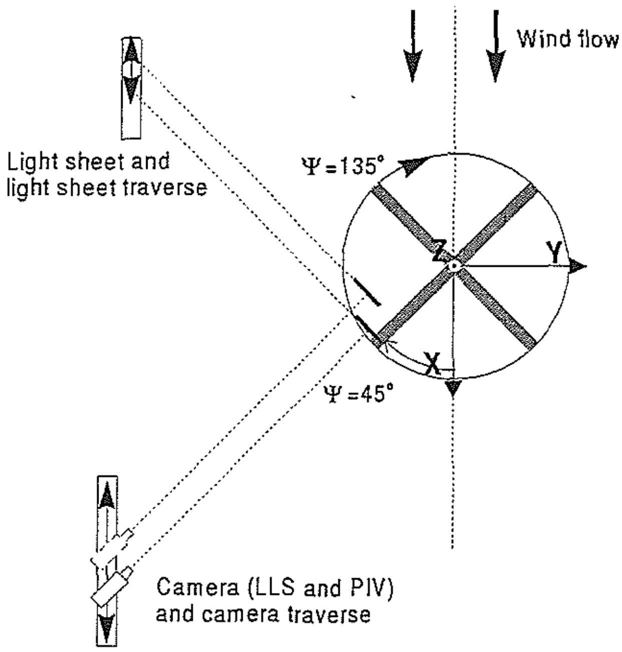

Fig. 4: Test set-up for PIV and LLS measurements

3 Experimental Results

3.1 Acoustic Results

3.1.1. Moderate-to-high speed level flight (S1MA results)

S1MA wind tunnel tests have concerned moderate-to-high speed level flight, from 215 km/h ($\mu^* = 0.283$) to 360 km/h ($\mu^* = 0.463$). The tests have shown in particular that the BVI phenomenon was a major source of noise even for relatively high speeds (up to 290 km/h). At ICAO noise certification flight condition (260 km/h) and beyond up to 290 km/h the ERATO rotor provides acoustic gains whatever the lift and the rotational Mach number is. The highest gains (up to 7 dBA) are reached in cases where BVI is present. This indicates that the design of the ERATO rotor is highly efficient, even for BVI occurring in level flight at blade azimuths between 70° and 90°. For example, Fig. 5 presents the filtered (6-40 bpf) averaged time signatures of both rotors at level flight condition ($\mu^* = 0.283$) indicating typical BVI waveforms.

For the 7AD rotor, the signal is composed of a succession of three impulsive peaks (per blade) caused by blade-vortex interactions occurring on the advancing blade side. For the ERATO rotor, only one interaction seems to generate BVI noise. The acoustic pressure peak is about half of the 7AD ones. The corresponding decrease in noise level is 7.6 dBA.

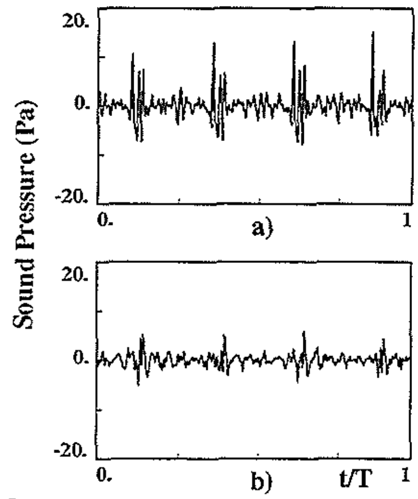

Fig. 5: 7AD - ERATO comparison at moderate speed level flight: $\mu^* = 0.283$, $Z_w^* = 15$, $M_{\Omega R} = 0.617$, a) 7AD rotor, b) ERATO rotor

The occurrence of BVI is confirmed by the analysis of the measured blade pressures (see sect. 3.2.1, Fig. 17). Three major interactions noted I1, I2 and I3 on Fig. 17 are clearly visible for the 7AD rotor, but just one major interaction (I2) on the ERATO rotor occurring at large blade azimuth.

The ERATO rotor also provides acoustic gains at high speed as illustrated in Fig. 6 which shows a comparison between 7AD and ERATO rotors at the maximum advancing tip Mach number attained by both rotors (M = 0.922).

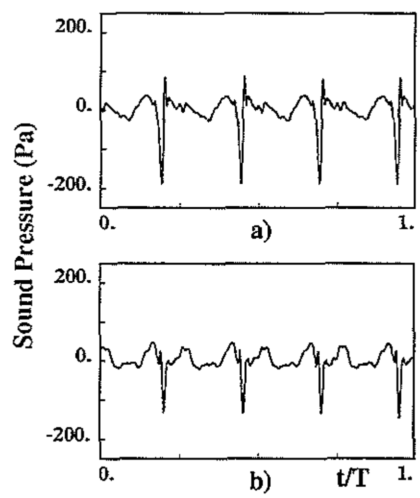

Fig. 6: 7AD - ERATO comparison at high speed level flight: $\mu^* = 0.423$, $Z_w^* = 15$, $M_{\Omega R} = 0.661$, a) 7AD rotor, b) ERATO rotor

This Mach number corresponds to the beginning of delocalization for the 7AD rotor. For this flight condition, the measured sound pressure level is 3.5 dBA lower for the ERATO rotor than for the 7AD rotor. This gain may be due to a shift of the delocalisation to a higher advancing tip Mach number for the ERATO rotor despite the ERATO blade tip geometry has not been optimised for high speed (contrary to the 7AD rotor with an optimised tip).

As a summary of the comparisons between both rotors, Fig. 7 shows the gains expressed in dBA calculated as difference between the maximum levels measured for the 7AD and ERATO rotors for increasing advancing speed.

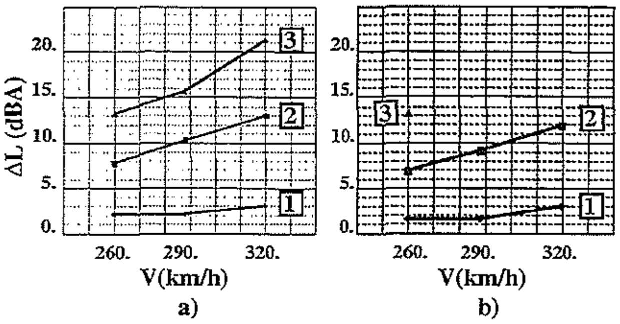

/1/: 7AD at $M_{\Omega R} = 0.661$, ERATO at $M_{\Omega R} = 0.661$
/2/: 7AD at $M_{\Omega R} = 0.661$, ERATO at $M_{\Omega R} = 0.617$
/3/: 7AD at $M_{\Omega R} = 0.661$, ERATO at $M_{\Omega R} = 0.573$

Fig. 7: 7AD-ERATO comparison in level flight, a) $Z_w^* = 12.5$. b) $Z_w^* = 15$

The comparisons between the two rotors are given for $Z_w^* = 12.5$ and $Z_w^* = 15$. One can notice that the ERATO rotor is quieter than the 7AD rotor for all the test conditions. The gains are close to 2 dBA at 260 km/h and 290 km/h ($\mu^* = 0.344$ and $\mu^* = 0.384$ respectively) and increase to 3 dBA at 320 km/h ($\mu^* = 0.423$).

The gains for the ERATO rotor increase up to 13 dBA for $\mu^* = 0.423$ when its rotational Mach number is set to its nominal value $M_{\Omega R} = 0.617$ (which is reduced compared to the nominal rotational Mach number of the 7AD, $M_{\Omega R} = 0.661$). Furthermore, it should be noted that the gain exceeds more than 20 dBA when the ERATO is operated at reduced tip speed corresponding to $M_{\Omega R} = 0.573$.

3.1.2 Low speed descent, climb and level flight (DNW results)

Acoustic results for the low speed descent range of the flight envelope, taken in the anechoic environment of the DNW, provide the basis for evaluating the BVI noise reduction potential of the optimised rotor.

Noise contours: In Fig. 8, the A-weighted sound pressure level contours for the 7AD reference rotor and the optimised ERATO rotor are compared for a range of flight path angles (• = +2° to -10°) rather than only at the check point of -6° at $\mu^* = 0.166$. The data were taken at the nominal reference condition for each of the two rotors, e. g. for a rotational tip Mach number $M_{\Omega R}$ of 0.661 for the reference rotor and of 0.617 for the optimised rotor at the reference advance ratio $\mu^* = 0.166$ and reference blade airload

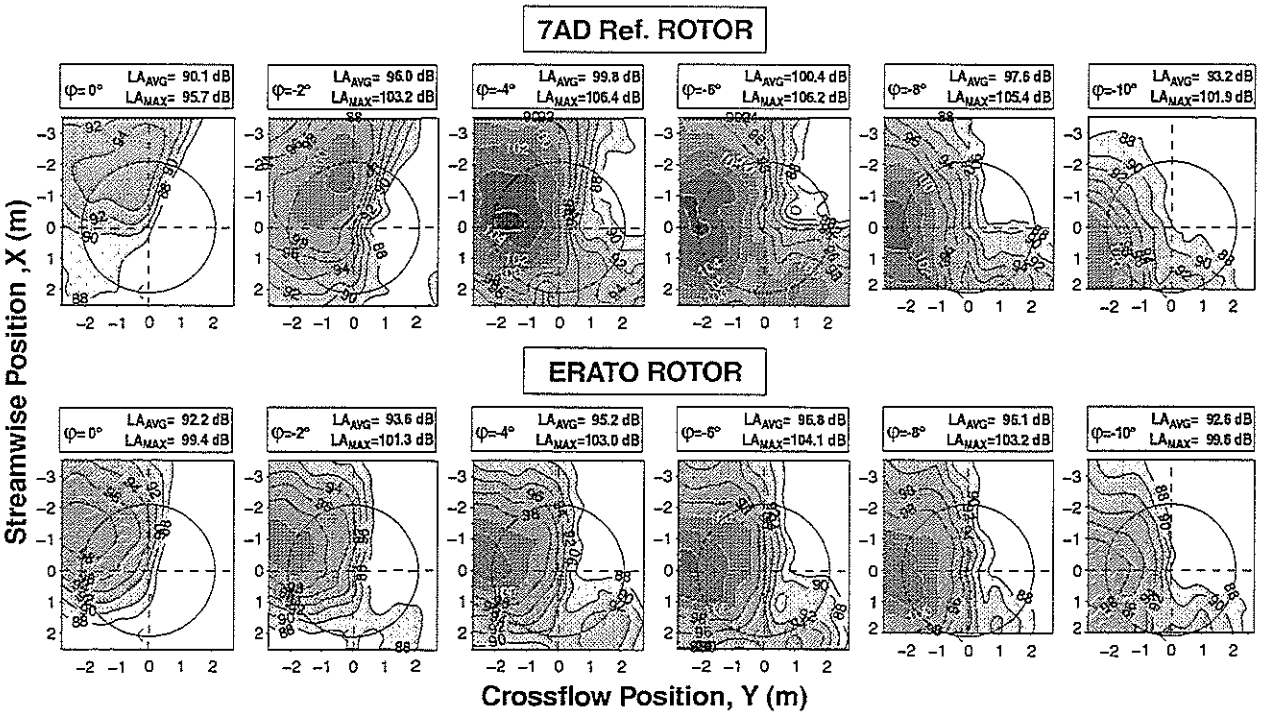

Fig. 8: A-weighted noise contours for 7AD reference and ERATO rotor for different descent angles at nominal reference conditions ($\mu^* = 0.166$ (V = 35 m/s), $Z_w^* = 12.5$)

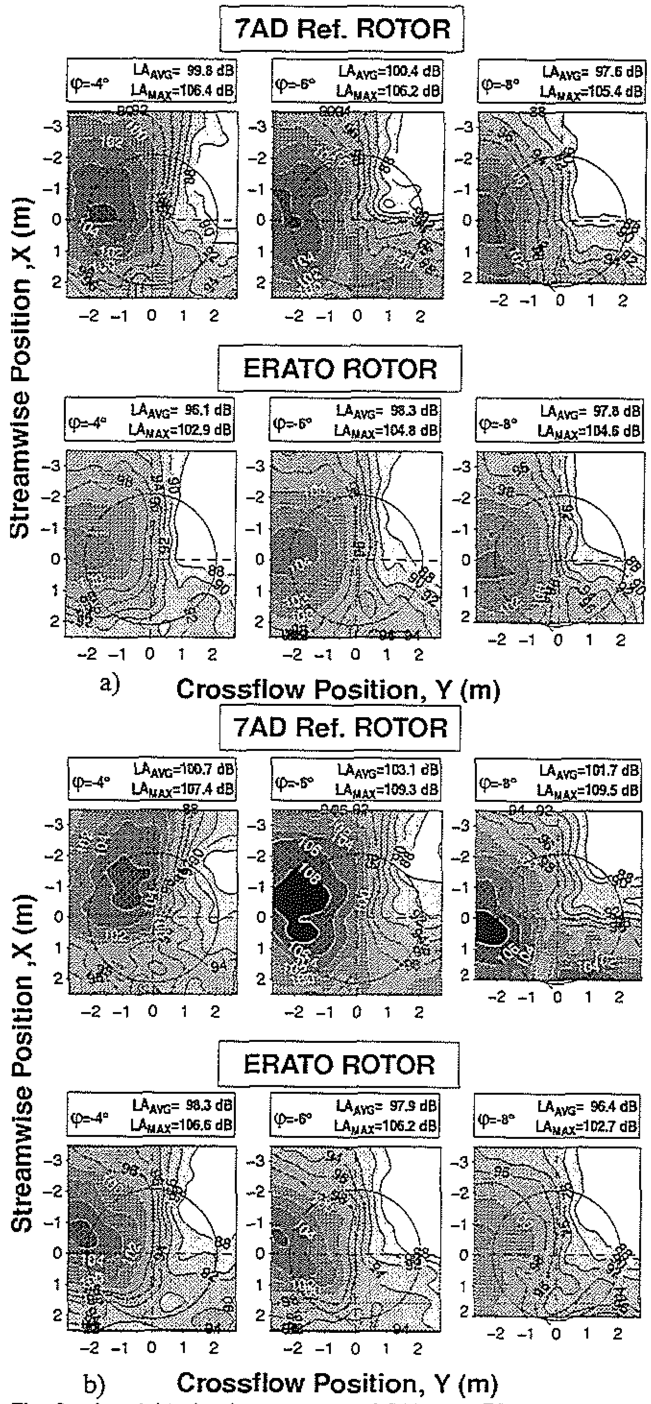

Fig. 9: A-weighted noise contours of 7AD and ERATO rotor for different descent angles (μ^* = 0.166), (a) at $M_{\Omega R}$ = 0.661 and Z_W^* = 12.5, (b) at $M_{\Omega R}$ = 0.617 and Z_W^* = 17.5 (high airload).

Z_W^* = 12.5. The comparison of the rotors at their nominal reference conditions is justified, since the rotational tip speed was one of the design parameters of the ERATO rotor. For the 7AD rotor intensive BVI noise radiation is observed in the descent angle range of 4° to 8°, which is seen dis- tinctly reduced by the acoustically optimised ERATO rotor, e. g. ΔLA_{MAX} = -2.1 dBA, ΔLA_{AVG} = -3.6 dBA for 6°-descent. At level flight (• = 0°), still low intensity BVI noise radiation is seen for both rotors, somewhat more intensive at the ERATO rotor. At higher descent angles (10° and 12°), significant noise reductions were obtained. Fig. 9 illustrates the BVI noise reduction potential when both rotors are operated at identical tip speeds and airloads. Optimum acoustic gains were attained at nominal tip speed of the ERATO rotor ($M_{\cdot R}$ = 0.617) and high blade airloads as shown in Fig. 9(b): ΔLA_{MAX} = -6.8 dBA, ΔLA_{AVG} = -5.3 dBA for 8°-descent.

Parametric Variations: The effect of blade airload variation on the noise radiation of both rotors is presented in Fig. 10, where spatial averaged A-weighted noise levels are plotted versus flight path angle, ranging from 2°-climb to 12°-descent flight at nominal advance ratio and tip speed. The noise reduction potential of the novel rotor is quite obvious.

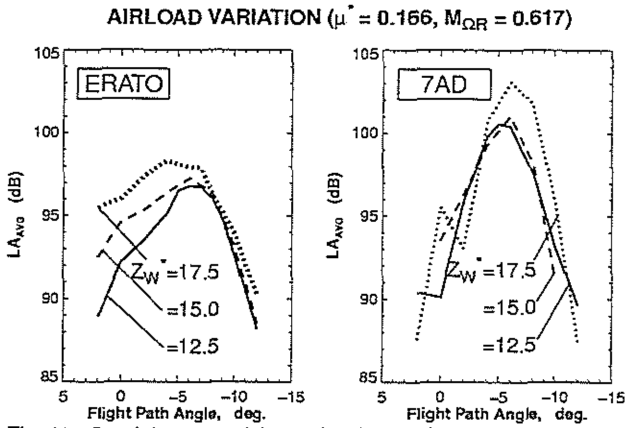

Fig. 10: Spatial averaged A-weighted noise levels (LA_{AVG}) versus flight path angle for variation of airload at fixed $M_{\Omega R}$ = 0.617 and μ^* = 0.166.

Furthermore, at higher descent angles, the ERATO rotor is acoustically much less sensitive to airload variations, while it is more sensitive at level flight and small descent angles. In Fig. 11 for both rotors the results of tip speed variation at nominal advance ratio and airload are provided. BVI noise radiation culminates between 5°- and 7°-descent.

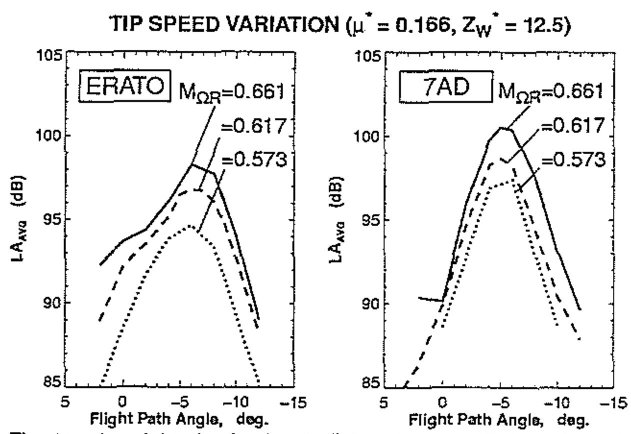

Fig. 11: A-weighted noise levels (LA_{AVG}) versus flight path angle for variation of tip-speed at fixed Z_W^* = 12.5 and μ^* = 0.166 (V = 35 m/s).

The spatial averaged noise levels are distinctly reduced for the ERATO rotor in this range and most significantly at the lowest tip speed measured. The effect of flight velocity on the sound field underneath the ERATO rotor in terms of LA_{AVG} is shown in Fig. 12. As found for other rotors (e. g. BO 105, 7A, 7AD), BVI noise generation is not restricted to low speed descent: similar BVI noise intensities were measured for higher velocities, but at different descent angles; it appears that the ERATO rotor is not very sensitive to airspeed variations.

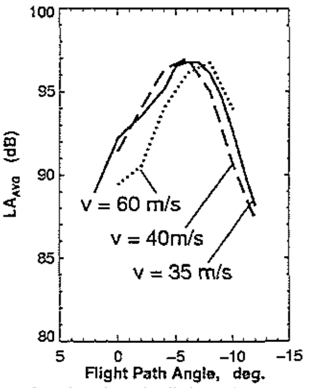

Fig. 12: A-weighted noise levels (LA_{AVG}) versus flight path angle for various airspeeds for the ERATO rotor at nominal conditions ($M_{\Omega R}$ = 0.617, Z_W = 12.5).*

The effects of blade lift and tip speed variations on the spatial averaged noise levels of selected flight conditions (corresponding to ICAO Annex 16 noise certification conditions) are shown in Fig. 13(a) and 13(b), respectively. In comparison to the 7AD rotor,

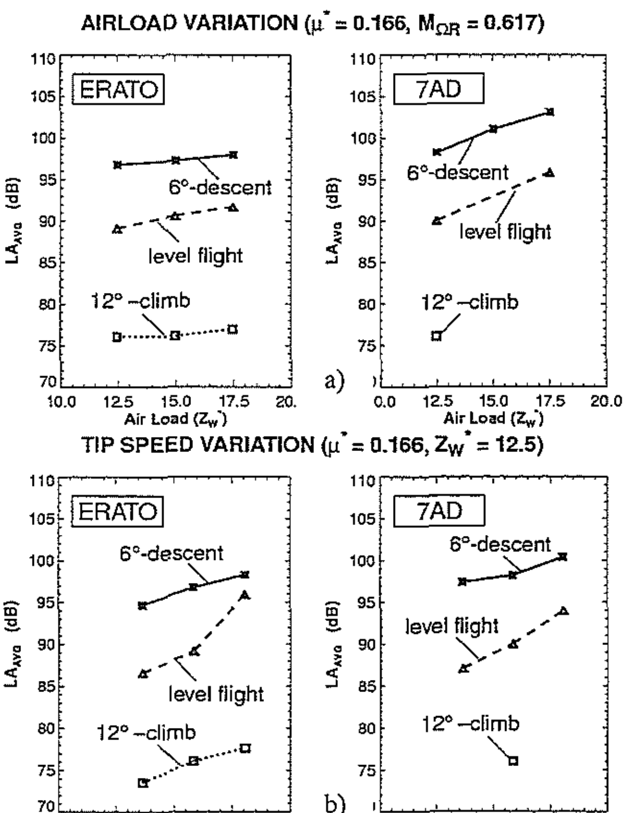

Fig. 13: A-weighted noise levels (LA_{AVG}) for airload variation (a) and tip-speed variations (b) at typical ICAO Annex 16, Chapter 8, flight conditions (6°-descent and climb at 35 m/s, level flight at 72 m/s)

the ERATO rotor appears to be less sensitive to airload variations for all three noise certification flight conditions comprising 6°-descent and (estimated) 12°-climb at 35 m/s (125 km/h) and level flight at 72 m/s (260 km/h). As seen in Fig. 13(b), both rotors are equally sensitive to tip speed variations. Except for 72 m/s level flight at high rotational speed, the ERATO rotor is generally quieter than the reference rotor at the noise certification test points. When compared at the nominal reference conditions of each rotor, a noise reduction benefit of 3.5 dB can be expected for level flight and descent and of about 1.5 dB for the take-off procedure.

Synthesis: The most important acoustic results obtained in the DNW test are summarised in Figs. 14 and 15, where in parts (a) the spatial averaged and in parts (b) the maximum A-weighted noise levels for both rotors are compared. As shown in Fig. 14 (a), the ERATO rotor operated at its nominal design lift (Z_w* = 12.5) and its nominal rotational speed of $M_{\Omega R}$ = 0.617 (210 m/s) is about 3.5 dBA to 5 dBA less noisy than the 7AD rotor operated at its nominal rotational speed of $M_{\Omega R}$ = 0.661 (225 m/s).

If the ERATO rotor is operated at a tip speed of $M_{\Omega R}$ = 0.573 (195 m/s), the noise reduction benefit is more than 6 dBA and the rotor is quieter than the 7AD rotor for all simulated flight path angles from 2° climb to 12°-descent. A similar statement is true for the maximum BVI noise radiation (Fig. 14(b)), however, the reduction in terms of ΔLA_{MAX} is somewhat less.

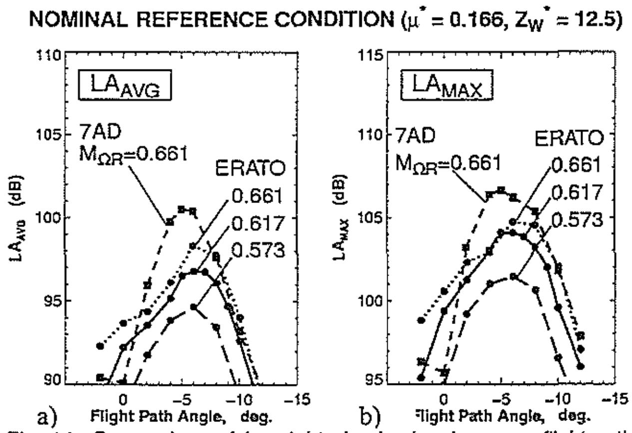

Fig. 14: Comparison of A-weighted noise levels versus flight path angle between 7AD rotor at nominal tip-speed and ERATO rotor at various tip-speeds (μ = 0.165, Z_W* = 12.5), (a) spatial averaged noise levels, (b) maximum noise levels.*

At higher lift (Fig. 15), when both rotors are compared at the same tip speed of $M_{\Omega R}$ = 0.617 (210 m/s), the ERATO rotor is less noisy than the 7AD rotor in a wide range of descent angles centered at 6°, with a maximum noise reduction of about 5 dBA for both the spatial averaged and the maximum noise level. Note that, if we compare to the 7AD rotor at its reference rotational speed of $M_{\Omega R}$ = 0.661 (using HELISHAPE test data, ref 14), maximum noise reductions of 7 dBA and more than 8 dBA

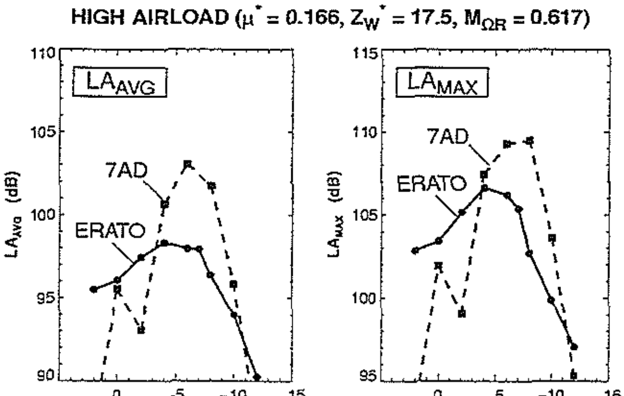

Fig. 15: Comparison of A-weighted noise levels versus flight path angle between 7AD and ERATO rotor at high airload (μ^* = 0.165, $M_{\Omega R}$ = 0.617, Z_W^* = 17.5),
(a) spatial averaged noise levels, (b) maximum noise levels.

appear attainable concerning the averaged and the maximum A-weighted sound pressure level, respectively. Altogether, one can state that the aeroacoustic design goal is globally satisfied.

3.2 Aerodynamic Results

3.2.1 Moderate-to-high speed forward flight (S1MA results)

The particular planform of the ERATO blade (with large local chord values inboard and low local chord values at the tip) was designed in order to try to reduce the tip vortex intensities. This has been checked using the blade surface measurements performed in S1MA. For each of the five instrumented sections, the pressure distributions were first integrated (in the chordwise direction) in order to calculate non-dimensioned airload coefficients $100C_nM^2c/R$. A Fourier analysis of these coefficients was then performed. The steady component of this analysis is plotted in Fig. 16 versus radius for the 7AD and the ERATO rotor for two test conditions: a moderate advance ratio (μ^* = 0.283) and a high advance ratio (μ^* = 0.423). In both cases, the airload

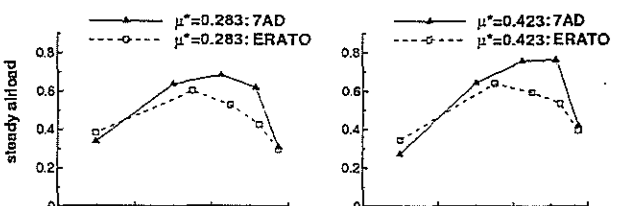

Fig. 16: Spanwise evolution of the steady components of non-dimensioned airloads ($100C_nM^2c/R$)

distribution on the ERATO rotor is more uniform than on the 7AD rotor and should lead to a reduction of the strength of the vortices emitted by the ERATO rotor. Furthermore, one can notice that the airloads in the outer part of the ERATO blade (r/R>0.7) are lower than on the 7AD blade and on the contrary are higher for the inboard sections, whatever the advance ratio is.

For moderate advance ratio (μ^* = 0.283), the analysis of the azimuthal derivatives of the leading-edge differential pressure coefficients ΔC_pM^2 allows to highlight the impulsive pressure fluctuations encountered by the 7AD blades due to Blade-Vortex Interactions. The contour plots of the $d/d\psi(\Delta C_pM^2)$ coefficients, plotted in Fig. 17, show three main advancing side interactions noted I1, I2 and I3 on the 7AD rotor.

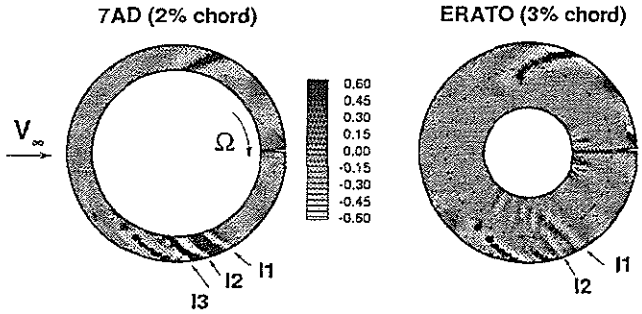

Fig. 17: Filtered (>10Ω) azimuthal derivatives of leading-edge differential pressure

On the ERATO rotor, the interaction noted I2 is the most impulsive but is much less intense than on the 7AD rotor. This analysis emphasises the existence of BVI even for moderate speed level flight (μ^*=0.283 corresponding to V_∞≈59m/s) and shows the significant reduction of the impulsiveness of BVI obtained thanks to the design of the ERATO blades.

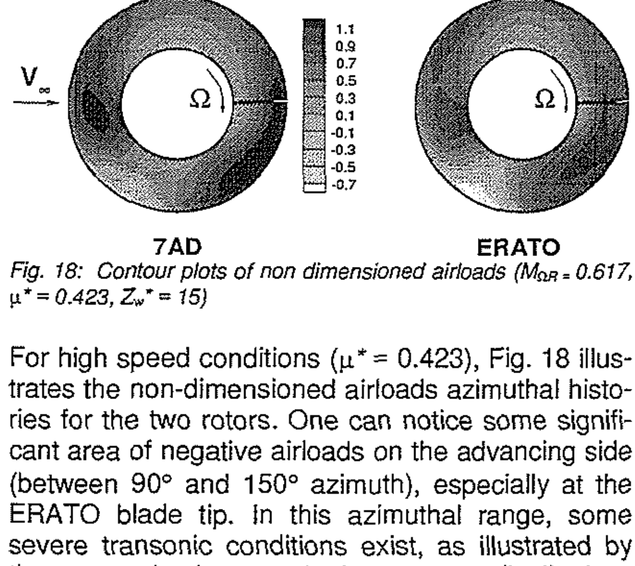

Fig. 18: Contour plots of non dimensioned airloads ($M_{\Omega R}$ = 0.617, μ^* = 0.423, Z_w^* = 15)

For high speed conditions (μ^* = 0.423), Fig. 18 illustrates the non-dimensioned airloads azimuthal histories for the two rotors. One can notice some significant area of negative airloads on the advancing side (between 90° and 150° azimuth), especially at the ERATO blade tip. In this azimuthal range, some severe transonic conditions exist, as illustrated by the strong shock waves in the pressure distributions of the two rotors (Fig. 19).

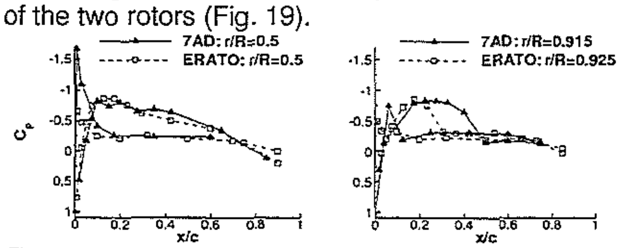

Fig. 19: Pressure distributions for ψ = 90° ($M_{\Omega R}$ = 0.617, μ^* = 0.423, Z_w^* = 15)

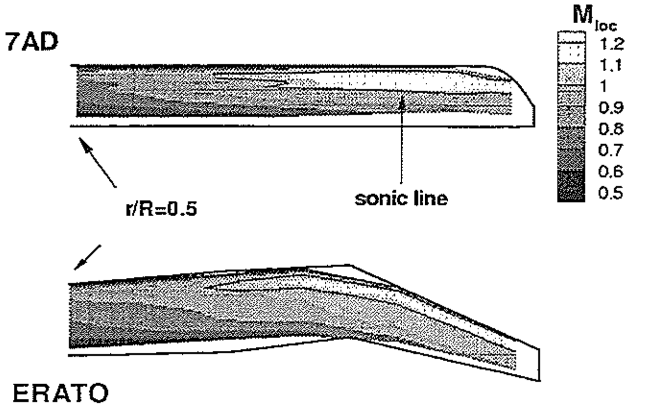

Fig. 20: Contour plots of local Mach numbers ($M_{\Omega R}$ = 0.617, μ^* = 0.423, Z_w^* = 12.5)

The contour plots of the experimental local Mach numbers (derived from surface pressure measurements) show a significant reduction of supersonic area on the ERATO blade compared to the 7AD blade (Fig. 20), mainly achieved thanks to the use of new generation airfoils OA3XX and OA4XX.

3.2.2 Descent and low speed level flight (DNW results)

BVI noise is generated through rapid pressure changes at and near the blade leading edge during vortex encounters. These are visible in the leading edge differential pressure time derivative contours given in Fig. 21. In descent (φ = -6°), the ERATO rotor exhibits fewer BVIs on the advancing side compared to the 7AD rotor. This suggests a reduced noise emission and indicates a steeper flight path of the vortices when penetrating the rotor disk, relative to the 7AD. The aerodynamic blade loading distribution in the same figure shows a larger dynamic content for the ERATO rotor in both level and descent flight. Compared to the 7AD, the maxima of the ERATO rotor loading are more focussed and in descent flight the 7AD blade has a small area at the tip between 125° and 180° azimuth with slightly negative loading. Measured by LLS and PIV, this negative airload was causing a double vortex system of opposite rotation similar to the one previously observed in the HART test (ref 8). The increased dynamic loading of the ERATO rotor may be compared to higher harmonic control effects, that can lead to steeper vortex flight paths within the rotor disk (as has been observed in the HART test).

The instantaneous radial circulation distribution at 140° azimuth is presented in Fig. 22 for level and descent flight at nominal condition (Z_w^* = 12.5) and in addition at the higher loading (Z_w^* = 17.5) in descent, where PIV data are available. In all these cases, the radial gradients of circulation at the outer 20% of the blade are smaller at the ERATO rotor, and the blade loading appears to be distributed more inboard compared to the 7AD. This is in agreement with one of the design ideas as already stated in section 3.2.1. As a consequence, the total circulation fed into the tip vortex will be smaller at the ERATO rotor.

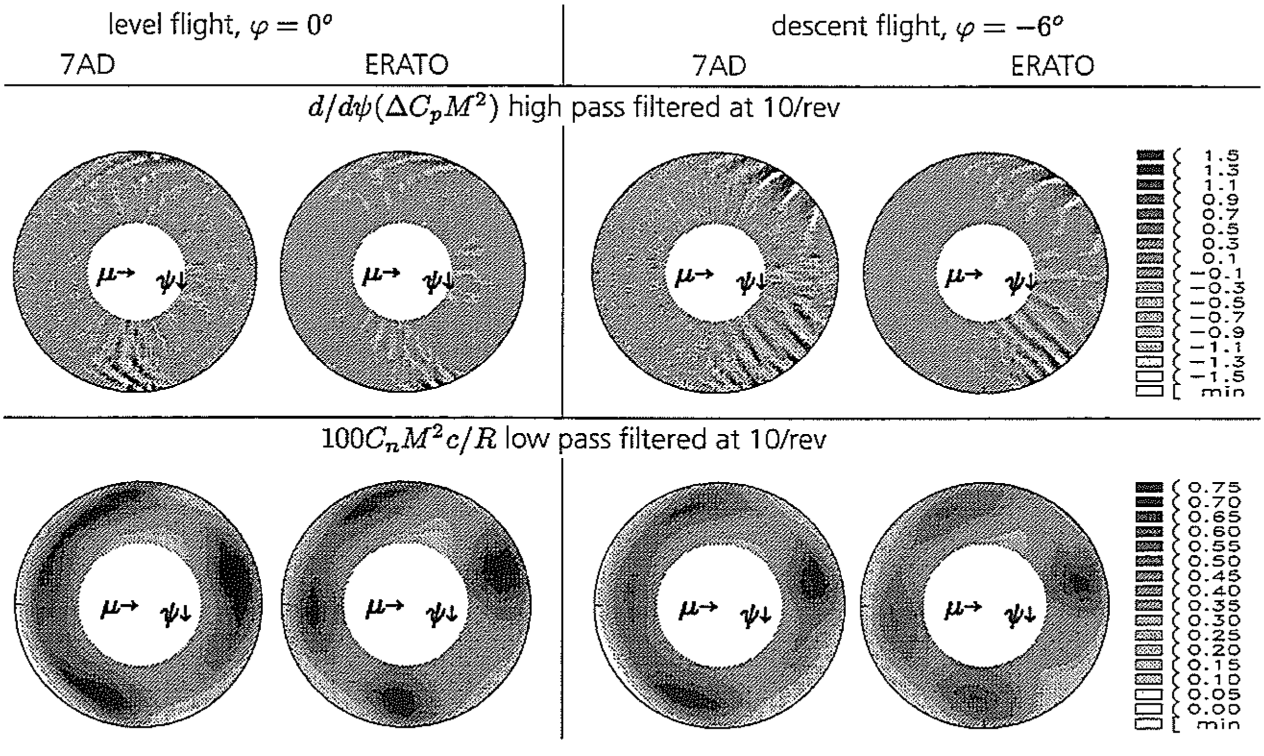

Fig. 21: Leading edge pressure (upper part) and aerodynamic loading distribution (lower part) of 7AD ($M_{\Omega R}$ = 0.661) and ERATO rotor ($M_{\Omega R}$ = 0.617) in level and descent flight, Z_W^* = 12.5, μ^* = 0.165.

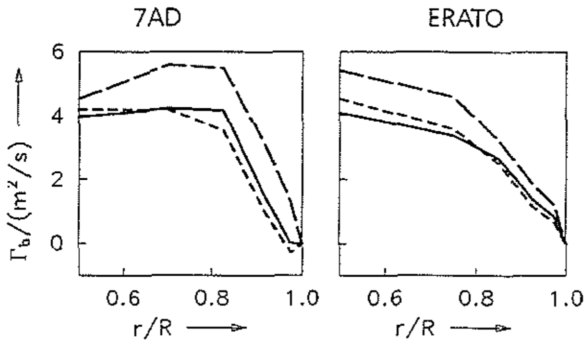

Parameters			7AD	ERATO
line	$\varphi/°$	Z_W^*	$M_{\Omega R}$	$M_{\Omega R}$
—	0	12.5	0.661	0.617
---	-6	12.5	0.661	0.617
--	-6	17.5	0.617	0.617

Fig. 22: Circulation distribution at • = 140° for various flight conditions of 7AD and ERATO rotor, μ^* = 0.165.

PIV measurements provide instantaneous velocity vector fields, from which the vorticity and circulation of the tip vortex can be calculated and analysed. Results for the high loading descent condition are given in Fig. 23. In agreement with the blade loading around • = 140° that was creating the vortices visible in the PIV data, the 7AD vortex is stronger than the ERATO vortex in both circulation and induced velocities, however, the peak vorticity ω_y is distinctly larger for the ERATO rotor.

The velocity profiles through the related vortex center position of 4 individual vortices and the geometric average is given in Fig. 24 together with the core radii and peak-to-peak velocities derived from these profiles. Although the ERATO core radii are smaller than the 7AD ones, the induced peak-to-peak velocity differences are smaller as well. It can also be recognized that a pure geometrical averaging of the individual PIV data (dashed line in Fig. 24) may lead to large errors in the experimental vortex properties. This indicates, that special averaging procedures are mandatory to obtain correct tip vortex velocity profiles.

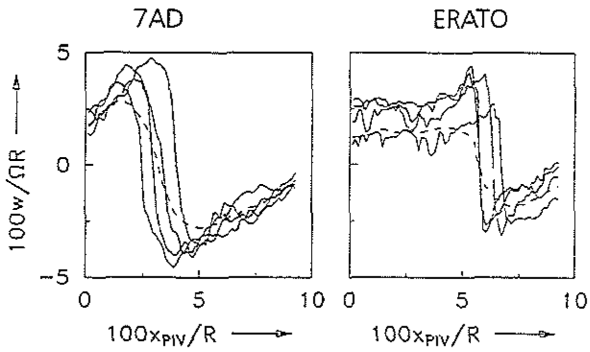

Vortex parameters:

no.	7AD $\frac{100 d_c}{R}$	7AD $\frac{100\Delta w}{\Omega R}$	ERATO $\frac{100 d_c}{R}$	ERATO $\frac{100\Delta w}{\Omega R}$
1	2.1	8.5	0.9	6.8
2	2.6	8.1	0.8	5.3
3	2.6	7.8	0.8	6.7
4	2.2	8.2	0.8	6.7
av	3.6	5.5	2.9	4.7

Fig. 24: Velocity profile through the vortex center of 7AD and ERATO rotor ($M_{\Omega R}$ = 0.617) in descent flight, φ = -6°, Z_W^* = 17.5, μ^* = 0.165. Each graph shows 4 individual and 1 average profile

The LLS flow visualisation technique has been applied to visualise and locate individual tip vortex cross-sections of the rotor wake pattern near the blade tip. Repeated application at shifted light sheets allowed to determine both tip vortex geometry sections and blade leading and trailing edge traces in space referenced to the rotor hub. A typical result is illustrated in Fig. 25 for the same low speed 6°-descent case at high airloads for which the PIV results (discussed above) have been obtained.

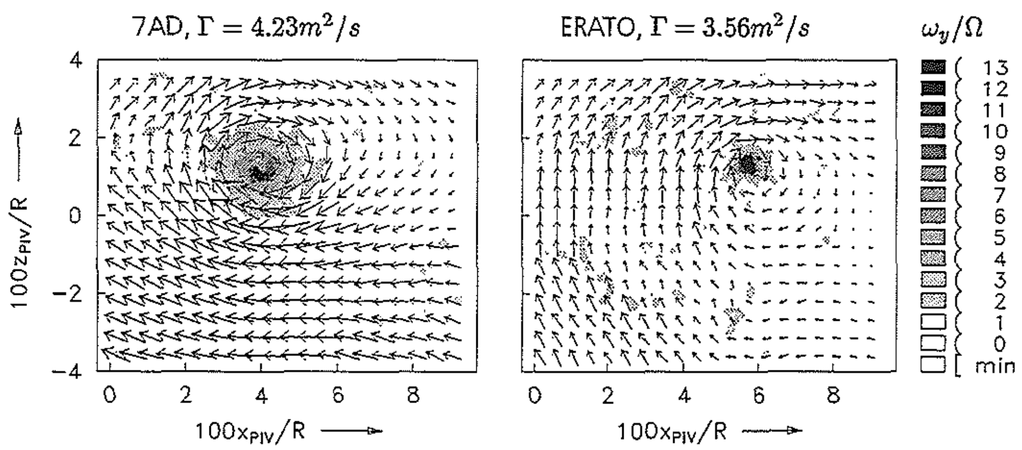

Fig. 23: Velocity vectors and computed vorticity of 7AD and ERATO rotor ($M_{\Omega R}$ = 0.617) in descent flight, φ = -6°, Z_W^* = 17.5, μ^* = 0.165.

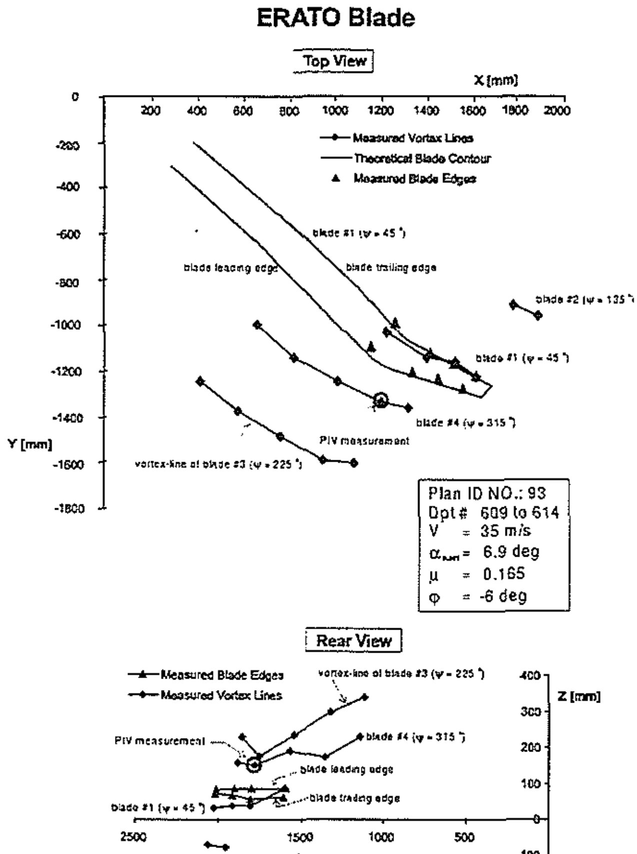

Fig. 25: Blade tip vortex sections and blade tip positions measured by LLS for 6°-descent at high airloads (μ=0.165, Z_W =17.5).*

Top view and rear view show the individual tip vortices generated by the four ERATO blades near the reference blade at 45° azimuth (a location where severe BVI occurs) and allow an estimation of the blade vortex miss-distance. The vortex being located at the trailing edge is seen directly cut by the blade. The location where the PIV measurement was conducted is indicated by the circles in Fig. 25. The LLS results, in general, will be widely used for detailed analysis of the wake predictions performed in the blade design process.

3.3 Aeromechanic Results

3.3.1 Moderate-to-high speed forward flight (S1MA results)

Rotor Performance: A typical example of the power consumed by the 7AD and ERATO rotors is illustrated in Fig. 26 for a tip rotational Mach number $M_{\Omega R}$ = 0.617. Whatever the advance ratio is, the ERATO rotor consumed much less power than the 7AD rotor. The power reduction can reach up to 12% for low thrust and high advance ratios, which is a very satisfying result. The power reductions seem to decrease for high thrust coefficients: however, there is still a power reduction of 4% for μ^* = 0.344 and Z_w^* = 12.5. Since one goal of the ERATO blade design was to consume not more power than the reference, the results obtained in S1MA show that this goal is reached and even largely exceeded.

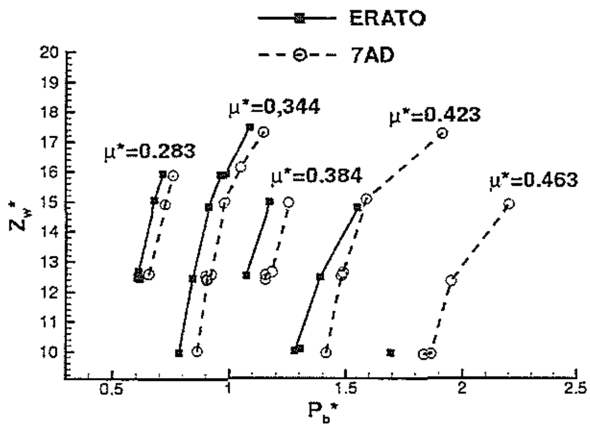

Fig. 26: Power consumption for $M_{\Omega R}$ = 0.617

Unsteady rotor deflections and vibration levels: One blade of each rotor tested in S1MA (7AD and ERATO) was equipped with strain gauge bridges (28 and 32, respectively). As an appropriate calibration had been performed in ONERA laboratory in Châtillon prior to the tests, the signals delivered by the gauges and recorded during the tests could be used thanks to the Strain Pattern Analysis to determine both unsteady flap and torsion deflection of the blades. The SPA also allowed to evaluate the 3-per-rev in-plane moment (in the rotating frame) and the 4-per-rev vertical shear. The main goal of the dynamic optimisation of the ERATO blade was that the in-plane moment should be reduced compared to that of the reference rotor (7AD) whereas the vertical shear should not exceed the reference level.

Fig. 27 shows the comparison between unsteady blade deflections (flap and torsion) for 7AD and

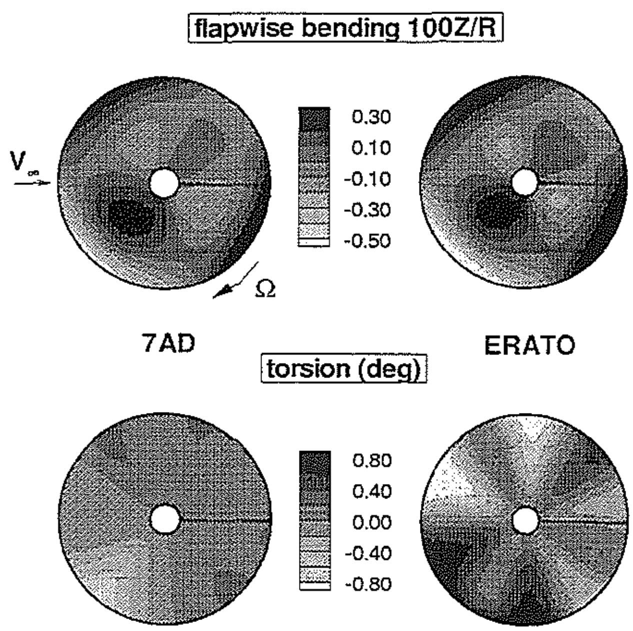

Fig. 27: Blade unsteady flap and torsion deflections ($M_{\Omega R}$ = 0.617, μ^* = 0.423, Z_w^* = 12.5)

ERATO rotors. It can be noticed that the two rotors exhibit very similar flap deflections, both in amplitude and phase. Concerning the torsion, the ERATO shows more harmonic content than the 7AD rotor. This can be traced to the fact that the rotating frequency of the second elastic flapping mode, which features a significant amount of coupled torsion, coincides with a harmonic of the nominal rotor speed, thus increasing the torsion content.

Fig. 28 presents a comparison of the 3/rev in-plane moment (blade root flap moment) in the rotating frame for 7AD and ERATO rotors with respect to advance ratio. The flight conditions are $Z_w^* = 12.5$, nominal rotation speed ($M_{\Omega R} = 0.617$), both rotors trimmed to zero flap angle. Although some penalties for the ERATO rotor can be noticed at low advance ratio (which was predicted by numerical simulations), an interesting decrease of the unsteady moment can be observed at higher speeds.

This illustrates that the main vibratory goal of the project has been achieved.

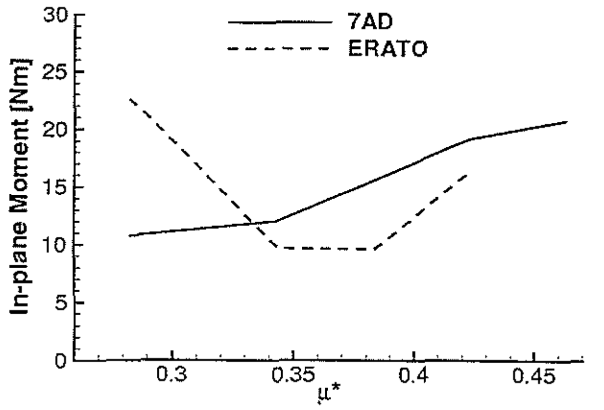

Fig. 28: In-plane moment evolution (3-per-rev component, $M_{\Omega R}$ = 0.617, Z_w^* = 12.5)

3.3.2 Descent and low speed level flight (DNW results)

From the bending moment distributions measured by strain gauges the elastic blade motion has been computed. Results are given in Fig. 29 for flap bending and torsion. As was already visible in the normal force distribution (Fig. 21), there is a pronounced dynamic torsion in 4/rev of the ERATO rotor, that is much larger compared to the 7AD. The reason for this behaviour is seen in the blade planform that introduces strong flap and torsion couplings, resulting in significant 4/rev torsion.

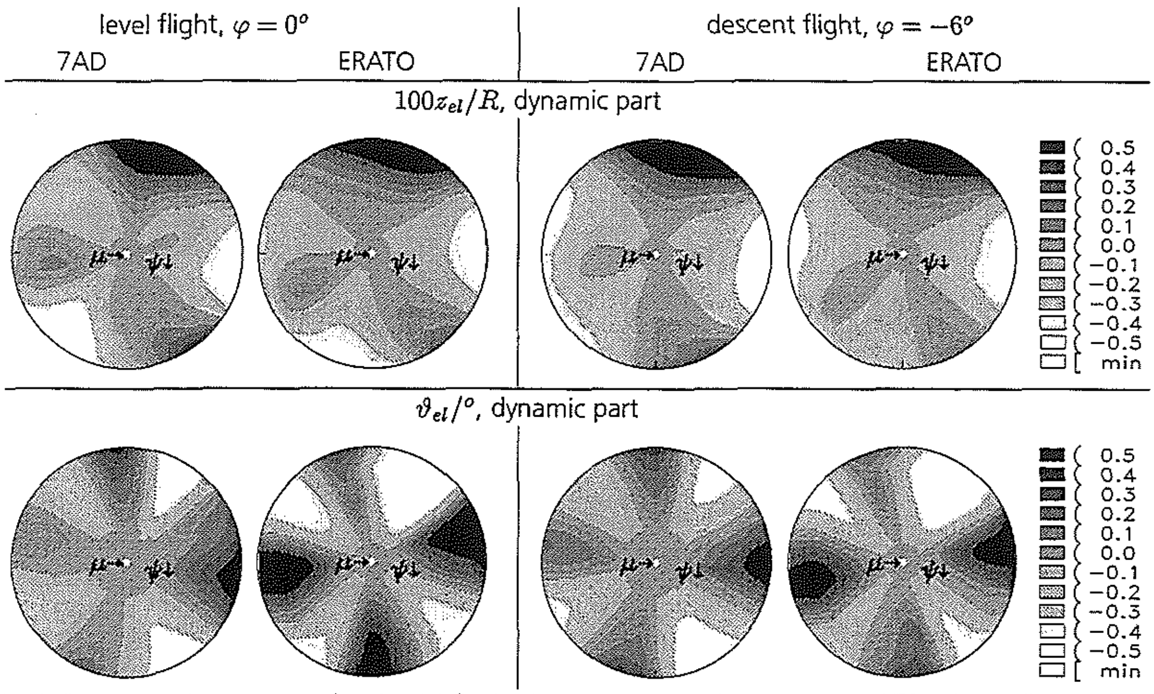

Fig. 29: Elastic flap bending (upper part) and torsional deflection (lower part) of 7AD ($M_{\Omega R}$ = 0.661) and ERATO rotor ($M_{\Omega R}$ = 0.617) in level and descent flight, Z_W^* = 12.5, μ^* = 0.165.

In Fig. 30 the 4/rev vertical blade root forces, representing a measure for vertical hub vibrations, are plotted versus descent angle for both rotors at its nominal operational conditions. Somewhat increased vibrations are seen at steep descent angles, while the vertical vibrations are lowered in the range below 6°-descent, at low speed level flight, and climb condition.

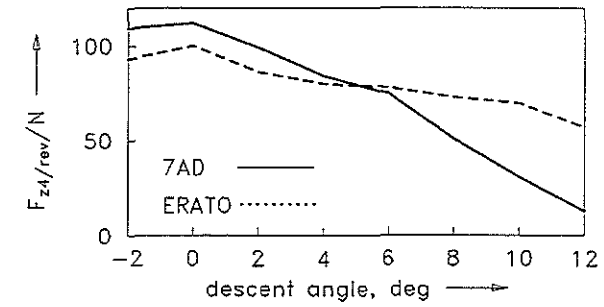

Fig. 30: 4/rev vertical blade root forces versus descent angle (μ^* = 0.166, $Z_W{}^*$ = 12.5, nominal $M_{\Omega R}$ of each rotor)

The initial analysis of the dynamic behaviour in low-speed descent flight indicates that there are no considerable penalties regarding vibrations in the fixed frame of the novel model rotor design at its nominal operational condition. However, for medium-to-high speed level flight, increased dynamic forces (dependent on tip speed) have been observed and need to be further investigated.

4 Conclusions

(1) The aeroacoustically optimised ERATO rotor provides in comparison to the 7AD reference rotor effective noise reductions *for descent flight at 35 m/s (125 km/h)* at the order of
- 3.5 to 5 dBA at nominal reference conditions
- 5 to 7 dBA at high airloads

and *for level flight at 90 m/s (320 km/h)*
- 12 to 13 dBA at nominal reference conditions.

(2) The acoustic gains are less impressive (2 to 3.5 dBA at descent and 1 to 2 dBA at level flight), when the ERATO rotor is operated at the nominal tip speed of the reference rotor. But, the gains are significantly increased (6 to 7 dBA at descent and exceeding 20 dBA at high speed level flight), if the rotational speed of the ERATO rotor is lowered to its minimum of 195 m/s.

(3) The BVI noise generation of the optimised rotor in descent flight indicates relatively low sensitivity towards descent angle (around 6°), airload (at steep descent), and flight velocity, which are important features for a real helicopter in landing approach.

(4) The ERATO rotor shows excellent aerodynamic performance at moderate-to-high speed level flight with power reductions from 4 to 12%, but limited to low-to-medium airloads. At low-to-moderate velocities, performance gains (up to 4%) were obtained for all airloads tested.

(5) The ERATO rotors' dynamic behaviour is not yet perfect. 3/rev in-plane moments in the rotating frame are slightly improved and for low speed descent, 4/rev vertical hub forces are of similar magnitude as for the reference rotor. But for medium-to-high speed level flight, the dynamic shear forces are higher compared to the reference rotor and depending on tip speed, a phenomenon requiring further analysis.

(6) Non-intrusive optical measurement techniques provided by DNW have been successfully applied to determine
- tip vortex geometry and blade-vortex miss-distance (via LLS)
- tip vortex strength and core size (via PIV)
- blade deflections in flap and torsion (via PGM, but not yet analysed in detail).

(7) In summary, the high quality experimental results globally verify the quiet rotor design methodology employed. These results also constitute a valuable data base which will help improving our physical understanding of BVI noise generation as a function of key aerodynamic and blade geometric parameters.

5 Acknowledgement

In tests of such extent and complexity, there are many people behind the scene who deserve high recognition for a job professionally and well done. The authors would like to offer their sincere thanks to their friends and colleagues at ONERA (Chatillon and Lille) and at DLR (Braunschweig and Göttingen) as well as to the test support teams of S1 Modane and of DNW, with special recognition of Edzard Mercker and Kurt Pengel for providing the non-intrusive optical measurement techniques.

The ERATO programme was supported by the French DGAC and the German BMBF.

6 References

1. Brentner, K. S. and Farassat, F.: "Helicopter noise prediction: the current status and future direction", *DGLR/AIAA 14th Aeroacoustics Conf.*, Aachen, Germany, 1992.
2. Beaumier, P; Spiegel, P.: "Validation of ONERA aeroacoustic prediction methods for blade-vortex interaction noise by HART test results", *51st Annual Forum of the American Helicopter Society*, Ft. Worth, TX, 1995.

3. Schultz, K.-J.; Lohmann, D.; Lieser, J.; Pahlke, K.: "Aeroacoustic calculation of helicopter rotors at DLR". Paper No. 29 in *AGARD.CP 552 Aerodynamics and Aeroacoustics of Rotorcraft*, 1994.
4. Kitaplioglu, C. and BVI Working Group: "A review of methods for the prediction of BVI noise", *Technical Specialists' Meeting for Rotorcraft Acoustics and Aerodynamics*, Williamsburg, VA, Oct. 1997.
5. Brooks, T. F.: "Studies of blade-vortex interaction noise reduction by rotor blade modification", *Proc. NOISE-CON 93, Noise Control in Aeroacoustics, Williamsburg*, VA, 1993.
6. Jones, H. E.; Burley, C. L.: "A study on the effects of tip shapes on rotor noise", *Technical Specialists' Meeting for Rotorcraft Acoustics and Aerodynamics*, Williamsburg, VA, Oct. 1997.
7. Brooks, T. F. and Booth, E. R. Jr: "The effects of higher harmonic control on blade-vortex interaction noise and vibration", *J. Amer. Helicopter Soc.* 35 (3), 1993.
8. Splettstoesser, W. R.; Kube, R.; Wagner, W.; Seelhorst, U.; Boutier, A.; Micheli, F.; Mercker, E. and Pengel, K.: "Key results from a higher harmonic control aeroacoustic rotor test (HART) in the German-Dutch wind tunnel", *J. Amer. Helicopter Soc.* 42 (1), 1997.
9. Splettstoesser, W. R.; Schultz, K.-J.; van der Wall, B.; Buchholz, H.; Gembler, W; Niesl, G.: "The effect of individual blade pitch control on BVI noise - comparison of flight and simulation results", Paper No. AC07, *24th European Rotorcraft Forum*, Marseilles, France, Sept. 1998.
10. Ben Zeev, O. and Chopra, I.: "Advances in the development of an intelligent helicopter rotor employing smart trailing edge flaps", *North American Conference on Smart Structures and Materials*, San Diego, CA, 1995.
11. Prieur, J.; Splettstoesser, W. R.: "ERATO - an ONERA-DLR cooperative programme on aeroacoustic rotor optimisation", *25th European Rotorcraft Forum*, Rome, Italy, Sept. 1999.
12. Mercker, E.; Pengel, K.; "Flow visualization of helicopter blade tip vortices - a qualitative technique to determine the trajectory and the position of the tip vortex pattern of a model rotor", Proceedings *18th European Rotorcraft Forum*, Avignon, France, 1992.
13. Raffel, M.; Willert, C.; Kompenhans, J.: "Particle Image Velocimetry - A Practical Guide", *Springer Verlag*, Berlin-Heidelberg, 1998.
14. Schultz, K.-J.; Splettstoesser, W. R.; Junker, B.; Wagner, W.; Mercker, E.; Pengel, K. ; Arnaud, G.; Fertis, D.: "A parametric wind tunnel test on rotorcraft aerodynamics and aeroacoustics (HELISHAPE) - test procedures and representative results", *The Aeronautical Journal of the Royal Aeronautical Society*, April 1997, pp. 143 - 154; paper also presented at *the 22nd European Rotorcraft-Forum*, Brighton, UK, Sept, 1996.